S. Elmore, A. J. Thornton, R. Scannell, A. Kirk, the MAST Team

Scaling of the scrape-off layer width in MAST L-modes by infrared thermography

Scaling of the scrape-off layer width in MAST L-modes by infrared thermography

S. Elmore, A. J. Thornton, R. Scannell, A. Kirk, the MAST Team

S. Elmore, A. J. Thornton, R. Scannell, A. Kirk, the
MAST Team

Scaling of the scrape-off layer width in MAST L-modes by infrared thermography

Scaling of the scrape-off layer width in MAST L-modes by infrared thermography

S. Elmore, A. J. Thornton, R. Scannell, A. Kirk, the MAST Team

Scaling of the scrape-off layer width in MAST L-mode plasmas as measured by infrared thermography

S. Elmore[1], A.J. Thornton[1], R. Scannell[1], A. Kirk[1] and the MAST Team[1]

[1] CCFE-UKAEA, Culham Science Centre, Abingdon, Oxfordshire, OX14 3DB, UK

Introduction

The power exhausted from a tokamak plasma is directed, via the scrape-off layer (SOL), towards plasma facing divertor targets that are designed to handle high heat fluxes. The width of the SOL is important for future device design since it plays a role in setting the magnitude of the parallel heat flux arriving at these surfaces and the distance that can be tolerated between the plasma edge and first wall materials. The well-established Eich equation [1,2] can be used to characterise the divertor heat flux profile as an exponential decay for the SOL width, λ_q, and a Gaussian spreading factor, S, due to diffusion around the last closed flux surface (LCFS) into the private flux region. The profile shape is given by:

$$q(\bar{s}) = \frac{q_0}{2} \exp\left(\left(\frac{S}{2\lambda_q \cdot f_x}\right)^2 - \frac{\bar{s}}{\lambda_q \cdot f_x}\right) \times \mathrm{erfc}\left(\frac{S}{2\lambda_q \cdot f_x} - \frac{\bar{s}}{S}\right) + q_{bg} \qquad (1)$$

Where f_x is target flux expansion, q_0 sets the peak heat flux, q_{bg} allows for a background and $\bar{s} = s - s_0$ and s_0 is the strike point location. In this work the divertor heat flux widths of MAST, L-mode, attached double null (DND) plasmas have been characterised using a long wave (7.6-9 μm) IR camera at the upper outer divertor. All measurements have been taken in a steady state period and transient effects that can affect the profile width, such as sawteeth, have been filtered out, see figure 1 for an example IR profile.

Figure 1 Typical IR profile for divertor heat flux from upper outer target of MAST

Based on a previous database of H-mode IR data [3], the profiles have been fitted with the Eich equation (1) over the range 3S to 7(λ_q+S) with filtering on χ^2 and manual inspection of the profiles ensuring good fits. The database spans an operational space of 0.08 T $\leq$ B$_{pol}$ $\leq$ 0.23 T, 0.405 T $\leq$ B$_T$ $\leq$ 0.408, 0.41 MA $\leq$ I$_P$ $\leq$ 0.91 MA, 8.8 m $\leq$ L$_\parallel$ $\leq$ 12 m, 0.87 x10^{19} m^{-3} $\leq$ $\overline{n_e}$ $\leq$ 4.6 x10^{19} m^{-3}, 0.22 MW $\leq$ P$_{SOL}$ $\leq$ 3.08 MW, 0 MW $\leq$ P$_{NBI}$ $\leq$ 3.1 MW, -2 mm $\leq$ δr$_{sep}$ $\leq$ 13 mm; where B$_{pol}$ is the poloidal magnetic field at the outboard midplane, B$_T$ is the toroidal magnetic field at the magnetic axis, I$_P$ is the plasma current, L$_\parallel$ is the parallel connection length calculated 10 mm outboard of the separatrix, $\overline{n_e}$
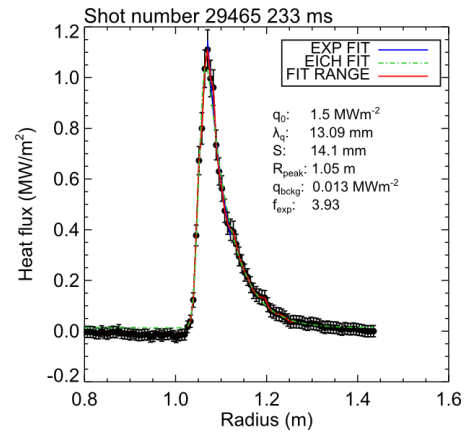
is the line averaged density, P_{SOL} is the power entering the SOL, P_{NBI} is the neutral beam heating power and δr_{sep} is the distance between the primary and secondary separatrix.

Results

Regressions of the SOL width have been performed on the L-mode database in the form $\lambda_q = C \cdot A^a \cdot B^b$, where C is a constant, A-B are plasmas parameters and a-b are the exponents of the fit. The regression uses a least squares fit in linear space and scaling parameters are chosen based on individual scalings found in the data and those used in previous MAST results [3,4]. Flux expansion is included in λ_q and calculated from the outboard midplane over the region R_{sep} to R_{sep} + 1cm.

Figure 2 Regression of measured λ_q with the most significant plasma parameters (I_P and $\overline{n_e}$)

The results from the regression can be seen in table 1, $\overline{R}^2$ is calculated as in [5]. In agreement with H-mode data from MAST and other machines, the strongest dependence is found on I_P; and equivalently B_{pol} and $L_\parallel$ when these parameters are used instead of I_P. The best quality regression can be seen in figure 2.
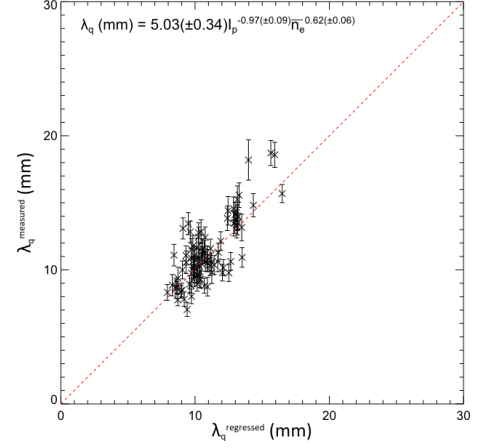
Table 1 Regression parameters for L-mode database

Reg.	Const.	I_P (MA)	B_{pol} (T)	$L_\parallel$ (m)	P_{SOL} (MW)	$\overline{n_e}$ ($\times 10^{19}$ m^{-3})	$\overline{R}^2$	χ^2
1	4.91±0.18	-1.04±0.06	−	−	0.03±0.02	0.60±0.03	0.57	4.25
2	1.21±0.17	−	-0.97±0.07	−	0.06±0.02	0.64±0.03	0.45	5.33
3	5.03±0.17	-0.97±0.04	−	−	−	0.61±0.03	0.57	4.24
4	0.89±0.12	−	−	0.92±0.05	−	0.51±0.03	0.41	6.01

The H-mode IR database from MAST [3] has been revisited to give a scaling with line averaged density and compared to the L-mode regression.

$$\lambda_q^{Hmode}(mm) = 3.63(\pm 0.63)I_P^{-0.75(\pm 0.11)}P_{SOL}^{0.24(\pm 0.04)}\overline{n_e}^{0.15(\pm 0.11)} \qquad (2)$$

Comparing the H-mode regression (eq. 2) with regression 3 from the L-mode database both show a strong scaling with I_P. The difference in density scaling is likely attributed to the limited range of densities in the H-mode database, since H-mode data is taken at densities most favourable for H-mode access. Most of the difference in the L- and H-mode scalings is in the regression constant coefficients; 4.91/3.63 ∼ 1.4; this is consistent with other machines that report $2\lambda_q^{Hmode} \geq \lambda_q^{Lmode}$ [6]. Previously Langmuir probe (LP) data has been used to generate scalings of λ_q [4]. The best match to the data in [4] is a regression using $L_\parallel$, and the separatrix density, n_e^{sep}, as measured by Thomson Scattering. The separatrix is defined as

where $T_e = 20$ eV; modelling on MAST shows the separatrix temperature is a typical value in L-mode across a range of different discharges, as in AUG [7].

$$\lambda_q^{IR}(mm) = 56.5(\pm5.38)L_\parallel^{0.36(\pm0.03)}P_{SOL}^{0.1(\pm0.02)}n_e^{sep\,0.10(\pm0.02)} \qquad (3)$$

With the regression shown in eq. 3 the exponent on $L_\parallel$ is consistent with that reported in [4]. A comparison of the regressions for the IR and LP L-mode databases is shown in figure 3. There are some discrepancies, particularly at higher valves of λ_q associated with low I_P where the LP data has a lower signal to noise than the IR. Another factor to consider is that the data taken from the LP measurements are from the lower divertor whereas the IR is measured at the upper divertor. It is possible that there is an effect from the magnetic geometry since L-mode double null plasmas in MAST are typically operated slightly shifted up, changing the balance of the upper and lower divertors. To investigate the effect of the magnetic configuration in MAST, IR data from lower single null (LSN) and DND plasmas have been compared at the lower outer divertor. Previous results from MAST [8] showed a dependence of λ_q with the sign of δr_{sep}. Data shown here, see figure 4, supports this effect, however the large scatter is due to variation in the plasma current in both LSN and DND. S/f_x shows no scaling with δr_{sep}. A comparison between

Figure 3 Comparison of LP and IR regressions using the IR database plasma parameters.

Figure 4 Variation of λ_q with δr_{sep} in LSN and DND

magnetic configuration of both λ_q and S/f_x were performed with $L_\parallel$ however there is no strong scaling for either when the sign of δr_{sep} is constant. To draw further conclusions a dedicated study is needed at fixed I_P to assess the impact of changing $L_\parallel$ and this will be a key experiment with the MAST-U Super-X divertor.

L-mode measurements of S/f_x are of similar size to those measured by IR in MAST H-mode plasmas [3], in the range $2 < S/f_x$ (mm) < 8. Although no scaling with plasma parameters were found from the H-mode database in MAST; measurements in AUG [5] showed scalings with B_{pol} and density. When varying only one parameter, scalings of S/f_x were found as S/f_x $\alpha\ \overline{n_e}^{-1.2}$ and $S/f_x\ \alpha\ B_{pol}^{-1.1}$; consistent with AUG [5]. The ion gyro radius, r_g, is thought to play a role in size of S/f_x, assuming $T_i = T_e$, particularly at high temperatures or low magnetic
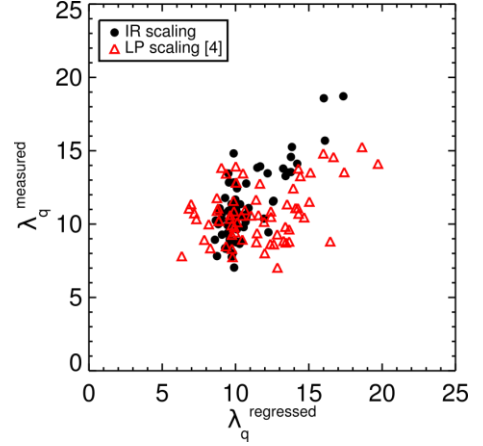
fields. MAST operates with a lower magnetic field in the divertor than conventional tokamaks, therefore a scaling of the following form was performed as in [5].

$$S = \frac{C_0 r_g}{f_x} + C_1 A^a B^b \ldots \qquad (4)$$

Regressions were performed both using eq. 4, and without the r_g contribution. The best regression of S/f_x can be seen in figure 5, which shows that the ion gyro radius dominates and there is a strong scaling with B_{pol} with a similar exponent to the λ_q results.

Figure 5 Best regression of S/f_x with plasma parameters

Conclusion

Scalings have been performed using IR data to determine which plasma parameters affect λ_q. Plasma current has been seen to have the strongest effect, as seen in previous work and other machines. The expected difference in L- and H-mode regressions is seen, consistent with other machines, and the difference is mostly due to the constant coefficient suggesting the dominant effect is increased transport. Comparisons to LP data give some similarities but a complete dataset with LP and IR analysed simultaneously is required to reconcile the differences and will be done in MAST-U in collaboration with MST1. Variation of λ_q and S/f_x is seen to only depend on the sign of δr_{sep} although the database is limited in the range of δr_{sep} at fixed I_P. The scaling of S is seen to depend on the ion gyro radius which can be larger in spherical tokamaks. In MAST-U the effect of the closed Super-X divertor will be studied to find the effect on scalings of λ_q and S.

Acknowledgements

References

[1] Eich, T., Phys. Rev. Lett. 107, (2011) 215001

[2] Eich, T., et al, Nucl. Fusion 53, (2013) 093031

[3] Thornton, A. J., at al., Plasma Phys. Control. Fusion 25 (2014) 055008

[4] Harrison, J. R., et al., J. Nucl. Mater. 438 (2013) S375

[5] Sieglin, B., et al., Plasma Phys. Control. Fusion 55 (2013) 124039

[6] Scarabosio, A., et al., J. Nucl. Mater. 438 (2013) S426-430

[7] Neuhauser, J., et al., Plasma Phys. Control. Fusion 44 (2002) 855

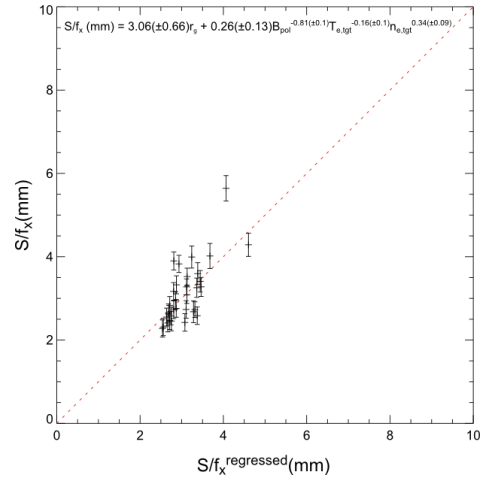[8] De Temmerman, G., et al., Plasma Phys. Control. Fusion 52 (2010) 095005